RESEARCH ARTICLE

Environment of severe storm formations over West Africa on the 26-28 June 2018

Marian Amoakowaah Osei[1,2,3] | Jeffrey N. A. Aryee[1] | Jacob Agyekum[1,4] |
Jesse Ashong[5] | Samuel Owusu Ansah[5] | Maureen Abla Ahiataku[5] |
Frank Baffour-Ata[6] | Leonard K. Amekudzi[1] |
Winifred Ayinpogbilla Atiah[1] | Michael Padi[7] | Johnson Ameho[7] |
Bashiru Yahaya[5,8,9] | Joseph Portuphy[5] | Benjamin Lamptey[5]

[1]Department of Meteorology and Climate Science, Kwame Nkrumah University of Science and Technology, Kumasi, Ghana

[2]Centre for Ecology and Hydrology, Crowmarsh Gifford, Oxfordshire, UK

[3]School of Earth and Environment, University of Leeds, Leeds, UK

[4]Water Research Institute, Centre for Scientific and Industrial Research, Accra, Ghana

[5]Department of Hydrometeorology, Ghana Meteorological Agency, Accra, Ghana

[6]Department of Environmental Science, Kwame Nkrumah University of Science and Technology, Kumasi, Ghana

[7]Safety Department, Air Navigation Service, Ghana Civil Aviation Authority, Accra, Ghana

[8]Complexity and Climate-Leibniz Center for Tropical Marine Research, Bremen, Germany

[9]Department of Earth Sciences, Jacobs University, Bremen, Germany

Correspondence
Marian Amoakowaah Osei, Centre for Ecology and Hydrology, Crowmarsh Gifford, Oxfordshire, OX10 8BB, UK.
Email: marianosans92@gmail.com and marose@ceh.ac.uk

Abstract

Understanding the environmental evolution of mesoscale convective systems (MCSs) is critical for forecasting weather in West Africa. This study investigated the thermodynamic and synoptic environments of MCSs over West Africa on 26 (storm 1) and 28 (storm 2) June 2018. Primary datasets used to assess the diurnal evolution of the storms were obtained from ERA5. The results showed a trapped gravity wave, enhanced by a well-established African Easterly Jet and monsoon trough, was responsible for the initiation of storm 1. Both storms also initiated in the presence of several moist lower (925–850 hPa) to mid-tropospheric (600 hPa) cyclonic and anticyclonic vortices, controlling inland moisture advection. The lower troposphere was moistened through moisture advection by the West African westerly jet for storm 1 and the nocturnal low-level jet prior to initiation for storm 2. For both storms, the evolution of outgoing longwave radiation showed a consistent atmosphere of deep afternoon convection. Boundary layer height increased significantly during storm evolution to support the increasing ascent of warm air. Vegetation cover differences may have also likely aided the evolution of storm 2. The passage of gravity waves from decaying storms can aid forecasters to nowcast likely regions of afternoon convection with high accuracy. Under the GCRF African Science for Weather Information and Forecasting Techniques (SWIFT), these findings are crucial in fulfilling the project's aims of improving weather forecasting capability and communication over West Africa.

KEYWORDS
atmospheric convection, boundary layer dynamics, GCRF African SWIFT, gravity waves, mesoscale convective systems

1 | INTRODUCTION

Intense well-organized mesoscale convective systems (MCSs) are the major products of the West African Monsoon (WAM) system. They are known to propagate in the order of hundreds of kilometres (Houze Jr, 2004; Parker & Diop-Kane, 2017), causing significant disruptions to socio-economic activities over the region. Their developments in the WAM are driven by both land–atmosphere coupling (Klein & Taylor, 2020; Taylor, 2008; Taylor et al., 2010) and synoptic features. Such that, over West Africa, strong gradients of moisture and heat occurring along vegetation boundaries induce a so-called 'vegetation breeze', which affects positively convection and storm initiations (Hartley et al., 2016). Similarly, large soil moisture gradients increase instability and enhance net radiation effect on surface energy partitioning, leading to MCSs intensification (Gu et al., 2006; Klein & Taylor, 2020). At the synoptic scale, deep convective heating across the inter-tropical discontinuity (ITD; airmass convergence zone) increases low-level baroclinicity, which strengthens the mid-level African Easterly Jet (AEJ). The consequence is the initiation of intense MCSs south of the jet. This AEJ also has the potential to trap atmospheric gravity waves (Plougonven & Snyder, 2005), which releases significant energy to destabilize the lower troposphere and trigger secondary storms (Halliday et al., 2018; Parker & Diop-Kane, 2017). According to Kafando et al. (2008), the energy associated with the initiation of these waves in the region is twice higher in the wet than dry seasons and is highly correlated with cloudiness and rainfall in the wet season.

The general knowledge of the thermodynamics and kinematics has shown that MCSs with the most intense convection occur in conditions of high lower tropospheric moisture, a drier mid-troposphere and stronger wind shear (Houze Jr, 2004). Yet, over the Sahel, event-based composites of 99 MCSs intensities positively correlate with weaker southerly winds, increased temperature and low relative humidity at 925 hPa and 700 hPa, respectively (Taylor et al., 2017). A strong lower-to-mid-tropospheric wind shear, on the other hand, may strengthen an MCS by increasing the updraft strength within the storm (Klein et al., 2021). This leads to storm anvils reaching higher altitudes relative to their level of neutral buoyancy (Baidu et al., 2022). Meanwhile, mid-tropospheric warming at the onset stage of convection can be quite detrimental to the formation of small convective clouds. However, this allows for the accumulation of more convective available potential energy (CAPE) in the boundary layer and the development of more intense systems once triggered (Parker & Diop-Kane, 2017).

To understand the complexity of the drivers of the WAM and organized MCSs, several studies have been undertaken over the years. Schrage et al. (2006) explored three MCS cases that occurred in different synoptic environments in 2002. Their results showed that the evolution of each storm ranged from moderately sheared and moist lower-to-mid-tropospheric moisture to a well-sheared and dry lower tropospheric moisture with low instability. Observations of 38 MCSs cold pools in Niamey showed a dynamic seasonal profile, with early season cold pools responsible for initiating secondary storms. Birch et al. (2013) assessed the importance of synoptic circulation, land-surface heterogeneities, and gravity waves on the initiation of MCSs using the highly resolved Met Office Unified model. They found that gravity waves emitted from a parent storm immediately initiated deep convection over regions with shallow convection and drier soils. Dieng et al. (2014) also found that strengthening of MCSs in Senegal was associated with the prior passage of the African Easterly Wave (AEW), which increased south-westerly flow and moisture advection. Studies over the Sahel have revealed a tripled frequency in MCSs initiations since 1980 in response to intense Saharan warming, which increased wind shear and induced changes to the Saharan air layer (SAL) (Taylor et al., 2017). Vizy and Cook (2018) found that MCS development occurs in hand with the ITD and is coupled with atmospheric pre-conditioning. Such that, growth of the planetary boundary layer from daytime surface heating and turbulent mixing enhances low-level wind convergence within 2°–3° south of the ITD. Bickle et al. (2022) showed that storms propagate with the speed of the AEJ and intensify from the inflow of convectively unstable air.

Although MCSs occur on the global scale, West African MCSs are notable for the large fraction of evaporative cooling below the 0°C isotherm in their trailing stratiform part (see Schrage et al., 2006). In light of this, the increasing complexity of the dynamics of West African storms, poses serious challenges to their predictability and evolution. Consistent studies in their evolutions driven by synoptic and micro-scale environments may improve weather forecasting in the sub-region. As such, we focus on exploring the thermodynamic and synoptic environment of extreme rainfall occurrences, which is at

the core of the Global Challenges Research Fund African Science for Weather Information and Forecasting Techniques project. Two events in particular are analysed in this study: one that initiated in Ghana on 26 June, organized and affected Senegal on 27 June, and a new storm over southern Ghana on June 28. The study examined the potential role of an observed gravity wave traversing across Ghana and the dynamics of moisture, winds and surface temperature, as well as the planetary boundary layer's prevailing conditions during storm formation and evolution. The remaining parts of the article are structured as follows: data and methods in Section 2, results in Section 3, discussions in Section 4 and finally the conclusions in Section 5.

2 | DATA AND METHODS

2.1 | Data sources

2.1.1 | CHIRPS dataset

The Climate Hazards Group Infrared Precipitation combined with Station data (CHIRPS) is a quasi-global gridded precipitation product, with a spatio-temporal resolution of $0.05° \times 0.05°$ from 1981 to present (Peterson et al., 2013). It combines data from various sources, such as in situ rainfall observations, global climatology and satellite estimates to produce rainfall at each time step (Funk et al., 2015). CHIRPS has been found to have a good agreement with observed rainfall over West Africa in studies such as Dembélé and Zwart (2016); Akinyemi et al. (2019); Atiah, Amekudzi et al. (2020); Atiah, Tsidu et al. (2020). CHIRPS daily rainfall data for all June 26–28 1981 to 2018 were used for case study analyses.

2.1.2 | ECMWF reanalysis fifth generation (ERA5)

ERA5 is a fifth-generation ECMWF atmospheric reanalysis of the global climate (Hersbach et al., 2020). It assimilates global observations with model data to produce a consistent dataset based on physical laws (Copernicus Climate Change Service (C3S), 2017). The datasets are quality controlled during the assimilation process, and physical principles allow for data estimate in locations where in situ observations are sparse. ERA5 produces hourly estimates of climatic variables on a global scale using a 4D-Var assimilation approach with a 31-km horizontal resolution and 137 vertical levels ranging from the surface to 0.01 hPa. In the present study, ERA5 hourly data of zonal

and meridional winds, air temperature, relative humidity (RH in %), specific humidity (q in $g\ kg^{-1}$), cloud liquid water content ($clwc$ in $kg\ kg^{-1}$), cloud ice water content ($ciwc$ in $kg\ kg^{-1}$), vertical velocity (w in ms^{-1}), top net short-wave radiation (SWR in Wm^{-2}), outgoing longwave radiation (OLR in Wm^{-2}), boundary layer height (BLH in metres (m)) and boundary layer dissipation (BLD in Jm^{-2}) were obtained for all 26–28 June 1981 to 2018 at a spatial resolution of $0.25° \times 0.25°$ longitude/latitude. In addition, we computed a variable called the 'vertical mixing (qw in ms^{-1})', which is the product of the vertical velocity (w) and the specific humidity (q, converted to dimensionless). The vertical mixing shows the depth of ascent or descent of moisture in the troposphere.

2.2 | Analysis method

In June 2018, two severe storms affected the countries of Senegal and Ghana on 27 and 28 respectively. Storm 1 (impact region: Senegal), initiated along the Ghana–Togo mountainous ranges on 26 June 2018 at 1200 UTC, and affected Senegal on 27 June around 1200 UTC. Similarly, storm 2 (impact region: southern Ghana), also initiated in the afternoon from the decaying southward branch of a parent storm north of the country. These storms caused severe damage to lives, properties and livestock. The synoptic state of each storm in the pre-convective environment was analysed using winds and RH profiles at 925 hPa, 850 hPa and 600 hPa at 1200 UTC. We also identified the monsoon trough (MT) and the core of the AEJ as the abrupt veering of the winds in the anti-clockwise direction at 850 hPa, and strong easterly windspeed between 10 and 15 ms^{-1} at 600 hPa respectively. Next, the findings for each storm were reported separately. For storm 1, the skewT, virtual potential temperature (θ_v), Scorer parameter [I^2, Equation (1)] and Brunt–Vaisala frequency [N^2, Equation (2)] were used to assess the stability of the lower troposphere to potential gravity wave trapping on 26 June, at the closest in-situ station (Koforidua; see location in Figure S1). Hovmoller diagrams showing the cross-section of moisture and zonal wind profiles over West Africa were computed and plotted for each storm.

In addition, the diurnal evolution of thermodynamic parameters of moisture, cloud liquid/ice content, vertical moisture transport, SWR, OLR, BLH and BLD were assessed and interpreted, based on the areal averages over West Africa (storm 1, between longitudes 18.5°W to 3°E and latitudes 4°N to 23°N) and Ghana (storm 2, between longitudes 3.5°W to 1.5°E and latitudes 4.5°N to 11.5°N). For timesteps with rapid variations in the

areal averages of a variable across specific longitudes, this is reflected in the resulting figures as abrupt vertical shifts. We also employed the standardized anomaly index on the rainfall and thermodynamic variables to determine the anomalies in the case study events. For rainfall, the standardized anomalies were computed on the daily timescale for 27 and 28 June by using the long-term mean (climatology from 1981 to 2018) of the rainfall records for Equation (3). Similarly, hourly standardized anomalies were computed for the thermodynamic variables using the hourly climatology (1981–2018) of each variable for Equation (3). The rainfall anomalies were interpreted using Table 1, whereas for the thermodynamic anomalies, values within $\pm0.99\sigma$ are classified as normal, and values above/below $\pm0.99\sigma$ are higher/lower than the normal (where σ is the standard deviation). All derived quantities such as the virtual potential temperature, Brunt–Vaisala frequency and equivalent potential temperature (theta-e) were computed using MetPy version 1.3 (May et al., 2022).

2.2.1 | Theory of trapped gravity wave

The evidence of trapped gravity wave propagation on 26 June was detected using the Scorer parameter [Scorer (1949), Equation (1)], given as follows:

$$I^2(z) = \frac{N^2}{(U-c)^2} - \frac{1}{(U-c)^2}\frac{d^2U}{dz^2}, \quad (1)$$

where U is the wind speed at various heights (z) and c is the speed of the wave, which was estimated from Figure S1, using the distance–time relation travelled by the wave based on the leading edge. Figure S1 was also drawn from the satellite imageries shown in Figure 3a–d. N^2 is the Brunt–Vaisala frequency given as follows:

$$N^2 = \frac{g}{\theta_v}\frac{d\theta_v}{dz} \quad (2)$$

with g as the gravitational acceleration and θ_v as the virtual potential temperature. In order to get a strong trapped wave, a wave guide between the ground and a tropospheric layer where waves decay strongly, and $I^2 < 0$ is usually sufficient.

2.2.2 | Standardized anomaly

The standardized anomaly index [SAI, Equation (3), Wallace and Hobbs (2006)] is a method used to standardize

atmospheric variables by assessing their deviations from the mean.

$$SAI = \frac{x'}{\sigma(x)}, \quad (3)$$

where x' is the departure of a variable (x) at a specific timescale (hourly, daily, seasonal, or annual) from its climatological value ($\overline{X}$). The standard deviation for the total observational record is denoted as σ. Based on Equation (3), rainfall severity can be classified using the categorization in Table 1.

3 | RESULTS

3.1 | Storm rain accumulation and anomalies

Figure 1a,b shows daily accumulated storm rain rate, and the corresponding standardized anomalies (Figure 1c,d) on 27 and 28 June 2018 over the impact regions (shown in red box). Over Senegal, rainfall totalled between 10 and 50 mm on 27 June (Figure 1a), and anomalously high to a maximum of 4σ above normal (extremely wet event, see Figure 1c and Table 1). In southern Ghana on June 28, the storm was more intense over the western coast, with a daily accumulation of 60 mm (Figure 1b). Meanwhile, the accumulated rainfall at the middle sector of Ghana was around 30–40 mm (Figure 1b). This rainfall amount was about 3σ above the normal (Figure 1d), also indicating an extremely wet event (Table 1). Based on these anomalies, it is revealed the severity of the storms at the impact regions. In Ghana, severe floods resulted in damages to properties on 28 June, whereas in Senegal, abrupt decrease in surface temperature and wind gusts associated with the passage of the storm induced the

TABLE 1 SAI ranges (in σ) and description (McKee et al., 1993)

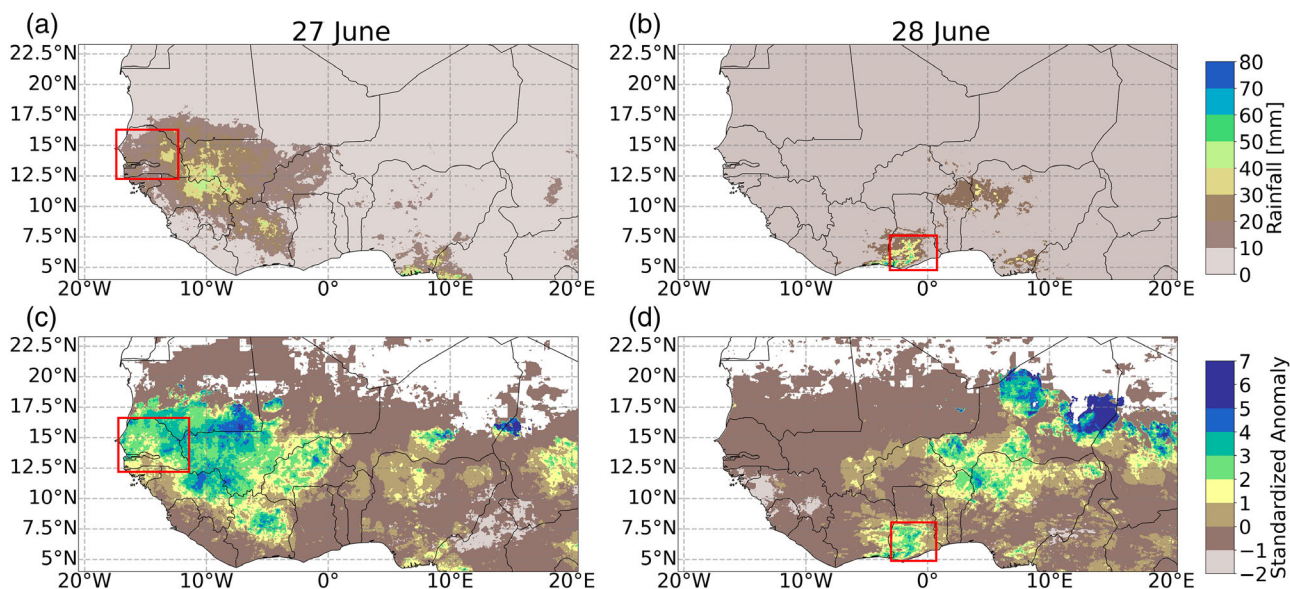| SAI range	Description
≥ 2.0	Extremely wet (EW)
1.50 to 1.99	Severely wet (SW)
1.00 to 1.49	Moderately wet (MW)
0.99 to -0.99	Near normal (NN)
-1.00 to -1.49	Moderately dry (MD)
-1.50 to -1.99	Severely dry (SD)
≤ -2.0	Extremely dry (ED)

FIGURE 1   CHIRPS storm rainfall accumulations on the (a) 27th and (b) 28th of June 2018. The corresponding standardized anomalies from 1981 to 2018 are found in panels (c) and (d). Red box denotes the area of severe impacts of each storm.

death of animals and damaged properties (Senghor et al., 2021).

3.2 | Synoptic controls: 26–28 June wind and moisture dynamics

At 1200 UTC on 26 June 2018, significant moisture (RH >60%) is observed below 15°N at 925 hPa (Figure 2a), with a corresponding cyclonic vortex ('C') over northeastern Niger. The moisture depth was also deep, extending from 925 hPa through to 850 hPa level (Figure 2d). The AEJ was established at 600 hPa (Figure 2g) with maximum wind speed of 10 ms^{-1}. The monsoon trough (MT) was also located at 850 hPa level, off the coast of Ghana (Figure 2d) and comparatively, south of the AEJ at 600 hPa (Figure 2g). On 27 June at 1200 UTC, RH increased above 80% over most regions below 15°N, with weak (2.5 ms^{-1}) moisture-laden southwesterlies and westerlies at 925 hPa (Figure 2b) level. These southwesterly winds filled into a series of cyclonic vortices ('C'), which were mostly located around 18°N (Figure 2b,e). At the time of storm 1's impact over Senegal (1200 UTC), these moisture-laden winds at 925 hPa (Figure 2b) from the Atlantic fed directly into the intensifying storm (red box in Figure 1a). The location of the AEJ core at 600 hPa is maintained through to 27 June (Figure 2h), while the MT is also positioned in central Cote D'Ivoire at 850 hPa level (Figure 2e). Typically, fast-moving MCSs propagate south of the AEJ core at 600 hPa, and northwest of the MT at 850 hPa level (Parker & Diop-

Kane, 2017). This orientation, as observed in Figure 2e,h was favourable for the extreme rainfall over all countries along the storm track towards Senegal on 27 June. For 28 June 2018, cyclonic vortices ('C') situated on the Senegalese coasts and inland over Mali at 925 hPa (Figure 2c) controlled southwesterlies at southern West Africa (Figure 2c), leading to an upsurge in moisture to 850 hPa level (RH >90%; Figure 2f). At 600 hPa level (Figure 2i), the AEJ core of about 10 ms^{-1} was maintained.

3.3 | 26-27 June 2018 (storm 1) analysis

3.3.1 | The role of trapped gravity waves on convection initiation on 26 June 2018

Prior to storm initiation on 26 June at 1200 UTC, a westward propagating atmospheric trapped gravity wave traversed the south of Ghana to Cote D'Ivoire between 0600 UTC and 2100 UTC (Figures 3a–d and S1). The wave developed from a decayed convective storm on 26 June 0000 UTC, along the coasts of Benin. At 1200 UTC, four convective cells had initiated at the upper flank of the wave over the Ghana–Togo mountain ranges (Figure 3c), growing rapidly by 1500 UTC (Figure 3d). Concurrently, the wave's leading edge had just traversed into Cote D'Ivoire, with new cells developing at the rear. The wave decayed at the south of Cote D'Ivoire at 1800 UTC (not shown), with a storm cell developing precisely at its leading edge. By this time, all the storms that had developed
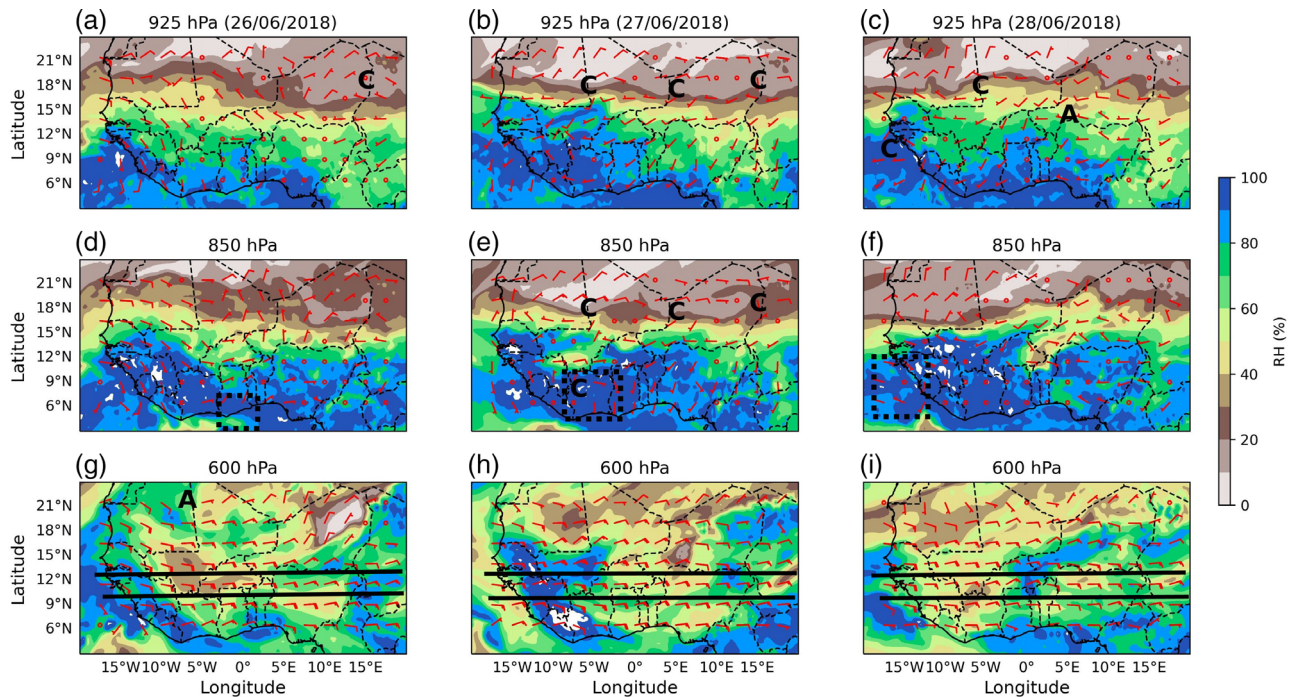
FIGURE 2   ERA5 winds and relative humidity (RH) over West Africa at the 1200 UTC for (a–c) 925 hPa, (d–f) 850 hPa and (g–i) 600 hPa levels from 26 to 28 June 2018. Areas with cyclonic and anticyclonic vortices are denoted with 'C' and 'A' respectively. Full wind barb has speed of approximately 5 ms^{-1}. In panels (d–f) is the evolution of the monsoon trough (MT) indicated in dashed square boxes, whereas the core of the AEJ is located between the black solid parallel lines in panels g-i.
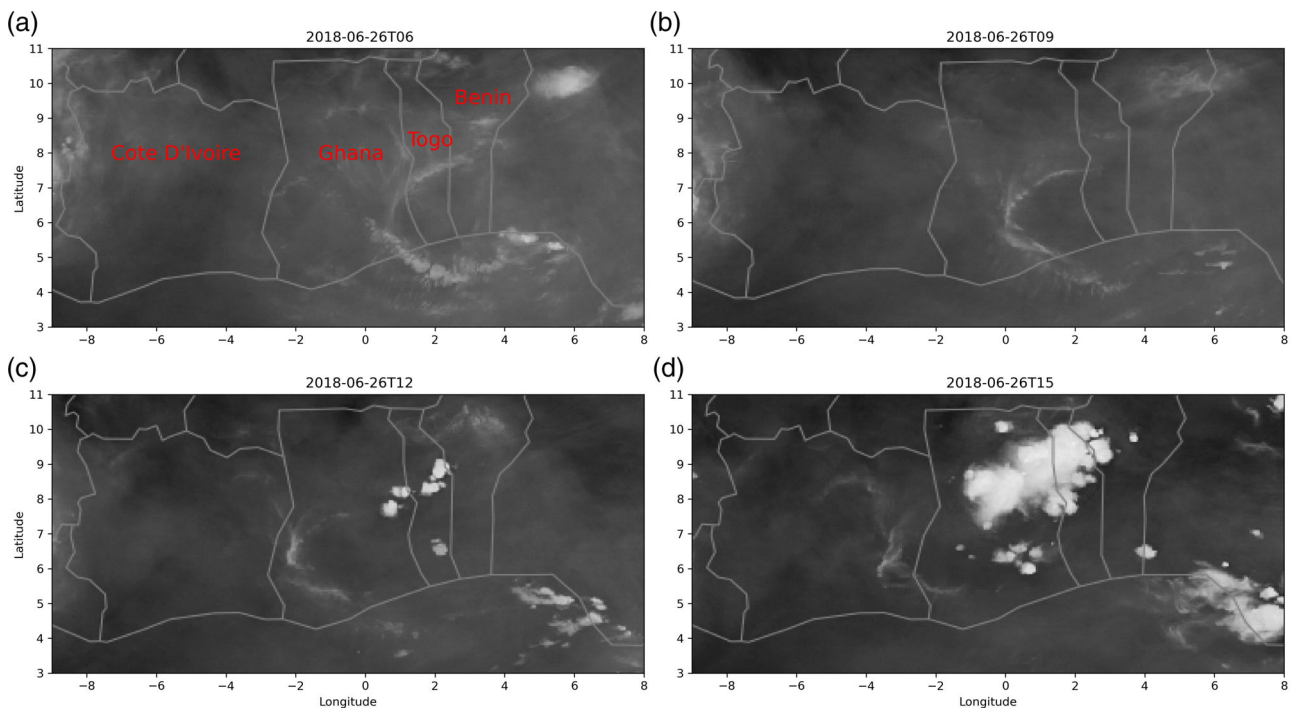

FIGURE 3   Propagation of an atmospheric wave across Ghana on the 26 June 2018 between 0600 and 1500 UTC. Imagery obtained from SEVIRI water vapour 6.2 channel 5. White and dark regions represent areas with the highest and lowest humidities, respectively. Notice the resulting deep convection at the rear of the wave from (c) 1200 UTC to (d) 1500 UTC. The countries traversed by the wave are annotated in red (panel a) as: Benin, Togo, Ghana and Cote D'Ivoire.

behind the wave had organized into a single MCS, with a northwestern track towards Senegal.

In Figure 4, we investigated the tendency of the troposphere to wave trapping. That is, we were interested in identifying a tropospheric environment that can support a wave guide between the ground and a layer where waves decay strongly. A stably stratified lower tropospheric layer, a Scorer parameter (I^2) < 0, a sudden decay of I^2 with height (preferably from the mid-troposphere), and the presence of a barrier is sufficient. In Figure 4a, there is evidence of a shallow layer of stability arising from residual night-time elevated SAL (region with the minimum value of dewpoint depression spread from 1000 to 800 hPa), which could support the formation of the wave at the low levels. The stability is further denoted by the increasing θ_v (Figure 4b) and $N^2 > 0$ (Figure 4c), which showed an overall high statically stable troposphere in the early morning. The implication of this tropospheric stability increases the possibility for a wave to travel along with the mean wind (U) into the upper troposphere, aided by the moderately strong low-level wind shear (below 700 hPa, Figure 4a). It follows that, if U varies with height inside the stable SAL layer (see Figure 4c), then waves of short horizontal wavelengths can become trapped (Stephan et al., 2021).
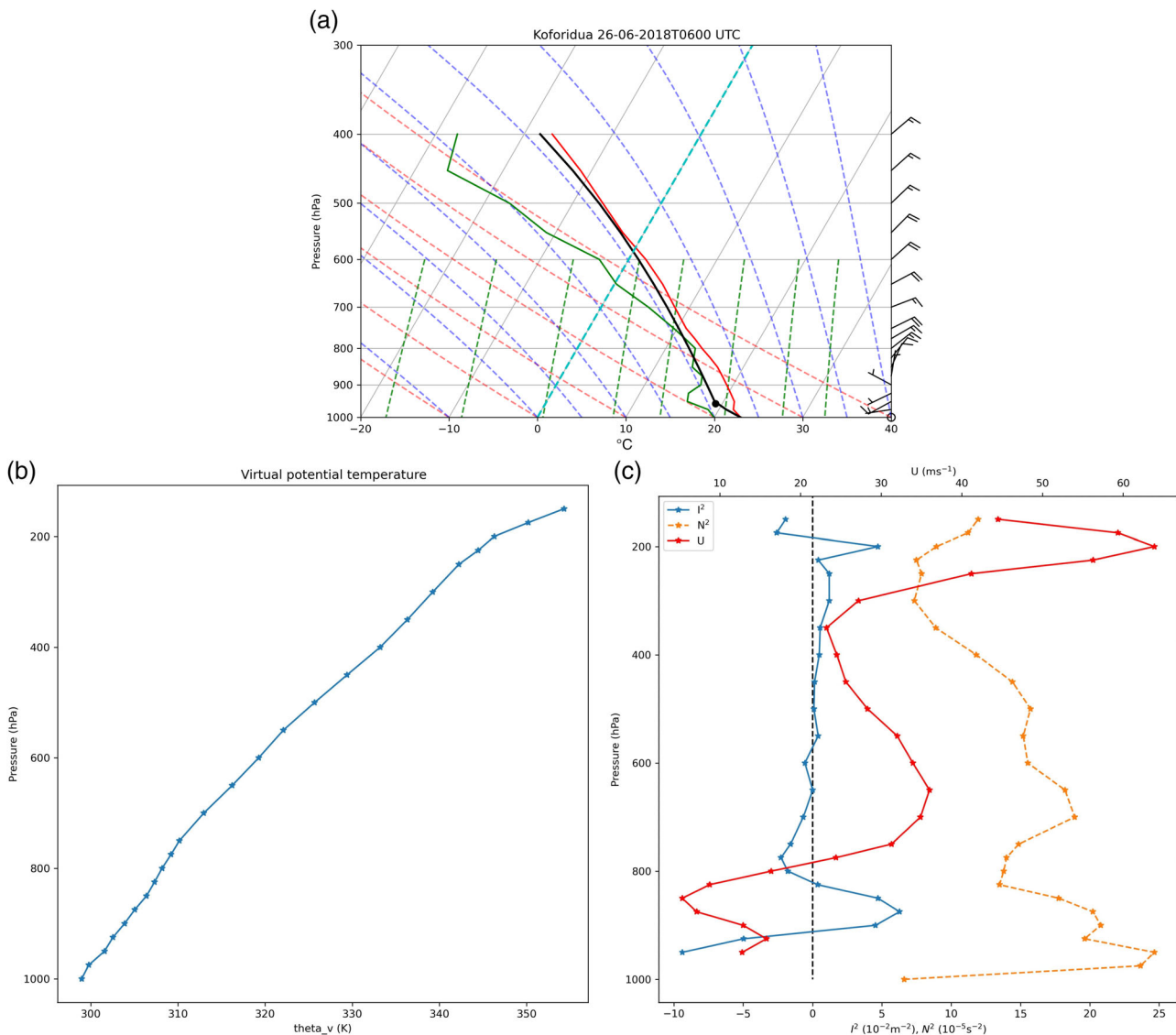

FIGURE 4 (a) SkewT profile at Koforidua, (b) virtual potential temperature and (c) the profile of the Scorer parameter (I^2), Brunt–Vaisala frequency (N^2) and mean wind speed (U) at 0600 UTC. ERA5 temperature at atmospheric pressure levels from 1000 hPa to 100 hPa was used to compute the virtual potential temperature, and the inclusion of zonal winds for Scorer parameter and Brunt–Vaisala frequency computations at Koforidua at 26-06-2018T0600 UTC. In addition, the various lines drawn on the SkewT include air temperature (solid red), dewpoint temperature (solid green), parcel profile path (solid black), temperature at lifted condensation level (black dot), zero degree isotherm (dashed turquoise), dry adiabats (dashed red), moist adiabats (dashed blue) and mixing ratio (dashed green). On the right side of the skewT are the wind barbs.

Additionally, the decay in I^2 should be such that, if it occurs suddenly at the mid-troposphere, it should divide the troposphere into two distinct regions; a lower layer with large values (high stability) and an upper layer with small values (low stability). This condition for I^2 is observed in Figure 4c, in which the sudden shift occurs around 600 hPa with very high (low) absolute values occurring below (above) 800 hPa. The 600 hPa level is also the climatological position of the AEJ, which served as the potential barrier needed to trap these waves (Crook, 1988; Kalashnik, 2013; Plougonven & Snyder, 2005; Wang et al., 2009). It is also crucial that the I^2 just around the AEJ be negative to increase the potential of trapping as observed in Figure 4c.

3.3.2 | Equivalent potential temperature

According to Oduro-Afriyie (1989), the troposphere becomes increasingly unstable when theta-e exceeds 320 K. In this study, therefore, we classified theta-e as stable (<320 K), marginally unstable (320–340 K), moderately unstable (340–360 K) and strongly unstable (>360 K). From Figure 5, storm 1 initiated in a region of moderate to high instability (theta-e, 340–370 K) at 925 hPa (Figure 5a) to 850 hPa (Figure 5b). Concurrently, over Senegal, the weak to moderately strong southeasterlies at 925 hPa (Figure 5a) and 850 hPa (Figure 5b) increased the moisture depth and instability. At 500 hPa (Figure 5c), the dry easterlies, veering to northeasterlies ($\approx$10–15 ms^{-1}), decreased instability to about 320–330 K at the region of storm initiation. All regions along the storm track (in blue box) also showed

high instability on the 26 June at 925–850 hPa (Figure 5a,b), which were significant for the initiation of secondary storms. During storm impact (27 June at 1200 UTC; Senegal), theta-e was moderately unstable at 925 hPa level (Figure S2a). This was supported by the weak and moist oceanic southerlies and southwesterlies ($\approx$2.5 ms^{-1}), changing to westerlies in Senegal (Figure S2a). The theta-e standardized anomalies at the initiation region ranged from normal at 925 hPa (Figure 5d) and 850 hPa (Figure 5e) to 1σ below normal at 500 hPa (Figure 5f) on 26 June (Figure 5). The corresponding wind speed anomalies were also extremely weak (less than 1 ms^{-1}, Figure 5d–f) over the entire West Africa. Wind anomalies on 27 June (Figure S2d–f) were similar to that of 26 June (Figure 5d–f); however, theta-e anomalies were about 1σ above normal in Senegal (Figure S2d–f).

3.3.3 | Diurnal evolution of atmospheric controls

The vertical cross-section of moisture and zonal winds averaged over longitudes 18.5°W to 3°E and latitudes 4°N to 23°N are shown in Figure 6. On both 26 and 27 June (Figure 6a–d), winds in the AEJ propagate westward with a speed of 10 ms^{-1} throughout the day. The nocturnal low-level jet (NLLJ, 2 ms^{-1} wind contours), was absent and played no role in storm initiation on the 26 June (Figure 6a–d). However, in the early hours of 27 June, a weakly established NLLJ advected moisture into the region, with depth from the surface to approximately
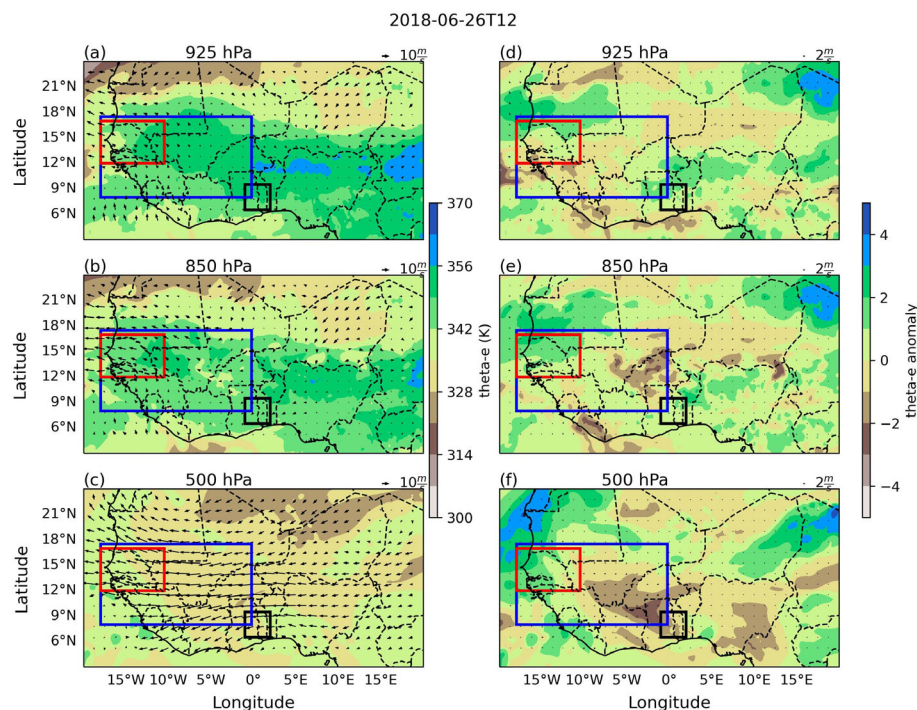

FIGURE 5 ERA5-derived equivalent potential temperature and wind vectors (a–c) and their standardized anomalies (d–f) on 26 June 2018 at 1200 UTC. The black box indicates the region of convective storm initiation on 26 June. The blue box in panels (a–f) indicates the propagation track for storm 1 between 26 June 1200 UTC and 27 June 1200 UTC. Storm devastating impact area (Senegal) is highlighted with a red box on 27 June (d–f).
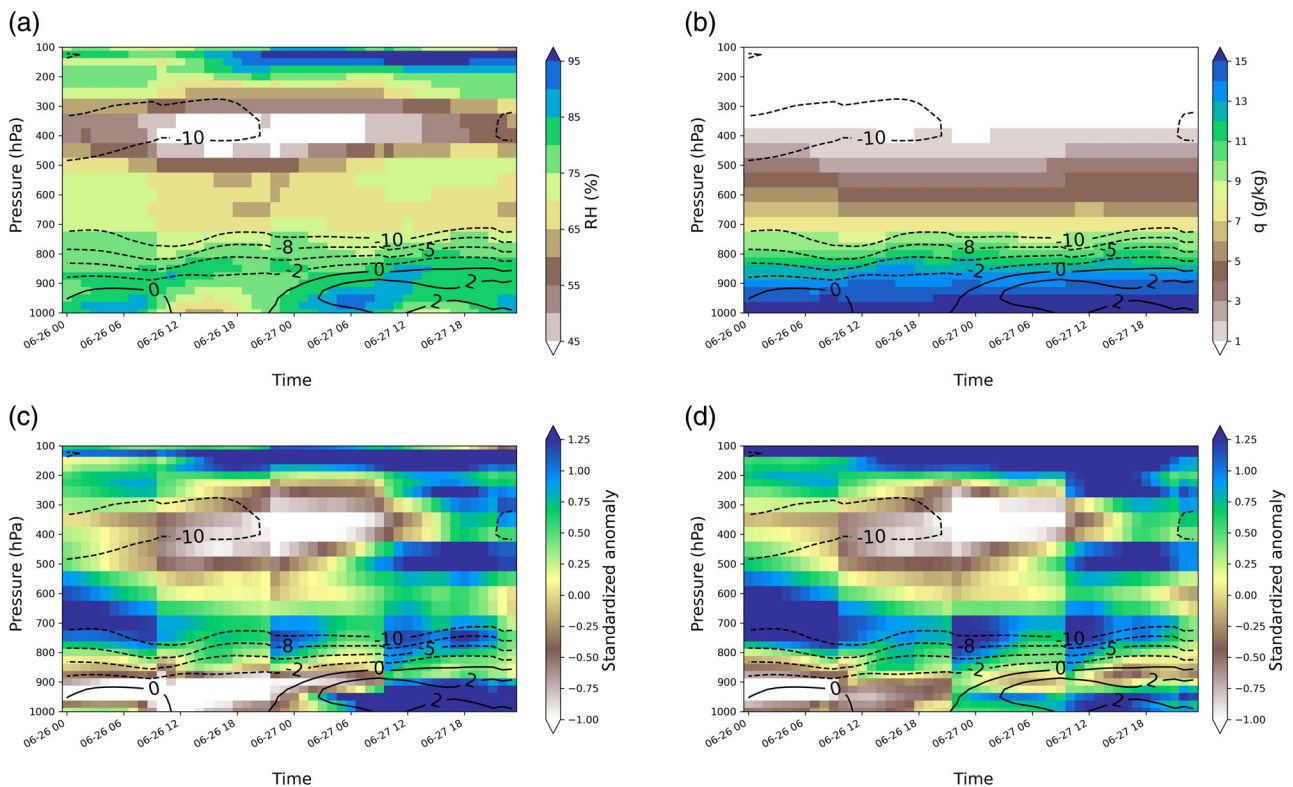
(a)

(b)

(c)

(d)

FIGURE 6 ERA5 diurnal vertical cross-section of (a) relative humidity, (b) specific humidity (c) hourly standardized anomaly of relative humidity and (d) hourly standardized anomaly of specific humidity averaged over longitudes 18.5°W to 3°E and latitudes 4°N to 23°N for 26 and 27 June 2018. Overlay of contour lines represents the zonal wind components. All times have units in the Universal Time Coordinate (UTC).

800 hPa (Figure 6a). This raised both relative and specific humidities at the low levels (1000–800 hPa) to about 80% (Figure 6a) and 16 g kg^{-1} (Figure 6b) respectively, and anomalies to around 0.25σ above normal (Figure 6c,d). The significance of the NLLJ on 27 June was likely to support the propagating storm with sufficient low-level moisture in the early hours of the morning.

Between 1200 and 1800 UTC on 26 June, the moderately high RH (60%) below 900 hPa (Figure 6a) was accompanied by moderate areal averaged vertical ascent (Figure 7a) at approximately 0.04 ms^{-1} (1000–500 hPa). Vertical ascent increased over the region, from the surface (1000 hPa) to the upper troposphere (200 hPa), with a maximum at 1200 UTC on 27 June (Figure 7a). The strong vertical ascent of about 0.10 ms^{-1} on 27 June indicated the location of the fully matured cumulonimbus cloud. The areal averages also showed that low-level (1000–800 hPa) tropospheric vertical mixing (Figure 7b) was at a maximum (−0.0008 ms^{-1}) between 27 June 1200–1500 UTC, with moderate mixing (−0.0006 ms^{-1} to −0.0002 ms^{-1}) extending to the mid-troposphere (500 hPa). At the same time, cloud liquid water content was high, up to 2.5 kg kg^{-1} from 1000–400 hPa (Figure 7c). The elevated cloud ice water content (Figure 7d), at the upper troposphere (200 hPa) on

27 June between 0600 and 1200 UTC (2.5 × 10^{-6} kg kg^{-1}), also likely signified the location of the matured storm.

3.3.4 | Net radiation and boundary layer dynamics

Figure 8 shows the SWR and OLR from 26 to 27 June 2018, averaged over West Africa. Two maxima in SWR (1000 Wm^{-2}) initiating around 1000 UTC on 26 June, at 4°N and 15°N are observed (Figure 8a). In the region of storm initiation (8°N), SWR was relatively high (600–900 Wm^{-2}, Figure 8a), and associated with a zone of deep convection between 1500 and 1800 UTC (OLR <180 Wm^{-2}, Figure 8b) on 26 June. According to Fontaine et al. (2008), OLR is usually capped at 240 Wm^{-2} to distinguish between deep convective regions and warm surfaces. The lower the OLR (≤240 Wm^{-2}), the deeper the convection at a location, in the presence of moisture and ascent. The OLR greater than 240 Wm^{-2} indicates a zone of warm land surface (Fontaine et al., 2008), as characteristic of the Saharan regions above latitude 18°N. The OLR was capped to about 240 Wm^{-2} at the impact region (12.5°-16°N) at 1200 UTC (27 June), which
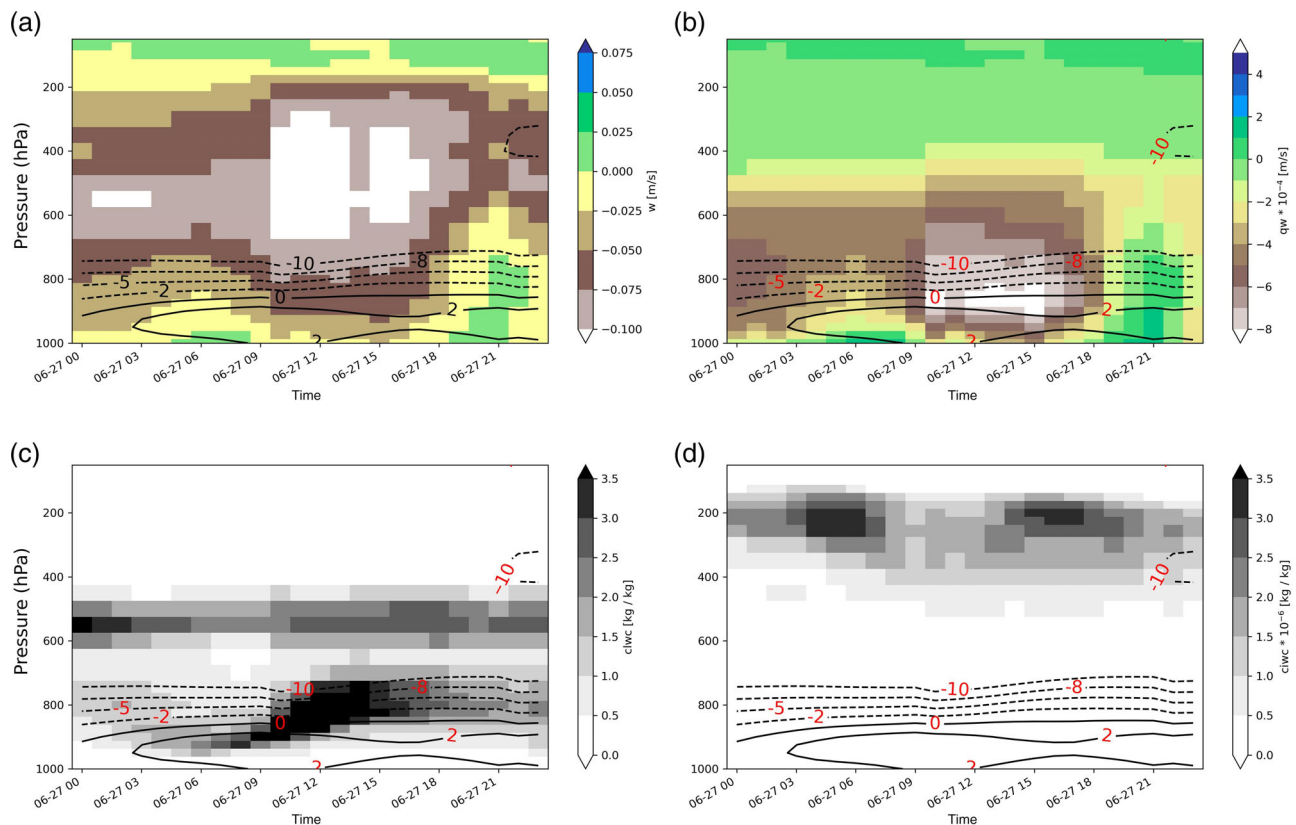
FIGURE 7 ERA5 diurnal vertical cross-section of (a) vertical velocity (*w*), (b) vertical mixing (*qw*), (c) cloud liquid water content (*clwc*) and (d) cloud ice water content (*ciwc*) averaged over longitudes 18.5°W to 3°E and latitudes 4°N to 23°N for 26 and 27 June 2018. Overlay of contour lines represents the zonal wind components. Negative vertical velocity denotes ascent of air, whereas positive values indicate subsidence. Additionally, the vertical mixing (b) is the product of the specific humidity and vertical velocity and shows the depth of ascent or descent of moisture in the troposphere. In panels (a–b), it follows that the more negative a value, the higher the vertical velocity or ascent. All times have units in the Universal Time Coordinate (UTC).

indicated the presence of the matured storm, with a decrease in deep convection. The OLR anomalies (Figure 8c) at storm initiation region (8°N, 180–220 Wm^{-2}; Figure 8b) on 26 June, and impact region on the 27 June (Senegal; 240 Wm^{-2}; Figure 8b) from 1200 to 1800 UTC varied from normal to 1σ above normal.

The boundary layer dynamics show a height of about 1200 m at the region of storm initiation ($\approx$ 8°N) on 26 June at 1200 UTC (Figure 9a). At the region of storm impact (12.5°N–16°N) on the same day (26 June), the boundary layer was deeper, extending close to 3000 m (Figure 9a). At both initiation and impact zones on the 26 June, these observed boundary heights were anomalously high, between 6σ and 11σ (Figure 9c). The anomalous increase in height was accompanied by large amounts of energy dissipated from turbulent activities (Figure 9b). In addition, rapid energy conversions from convection occurring at the storm initiation region (8°N, Figure 9b) on 26 June around 1200–1600 UTC reached a maximum of about 10,000 Jm^{-2}, and 5σ above normal (Figure 9d). On the 27 June, between 0900 and 1800 UTC, maximum energy dissipation is

located at the south (12.5°N–16°N; Figure 9b) of the maximum BLH (20°N–23°N, Figure 9a). This implies that the maturity of the storm over Senegal on 27 June at 1200 UTC may have been enhanced by the strong boundary layer turbulence as energy was driven into the storm from the Saharan region, coupled with the 925 hPa moisture advected by the westerlies and southwesterlies (see Figures 2a and S2a). In addition, the spatio-temporal location of the strongest areal averaged dissipated energy at 1500 UTC on 27 June (Figure 9b), coincided with the storm's latitudinal location over Senegal (12.5°N–16°N). Moreover, on 27 June, anomalies in energy dissipation at 12.5°N–16°N between 0900 and 1800 UTC were about 2–3σ above normal (Figure 9d).

3.4 | 28 June 2018 (storm 2) analysis

On 28 June 2018 at 1200 UTC, the southward moving branch of a decaying storm, which occurred over Burkina Faso and Niger, traversed over northern to southern Ghana. By 1500 UTC, this branch had
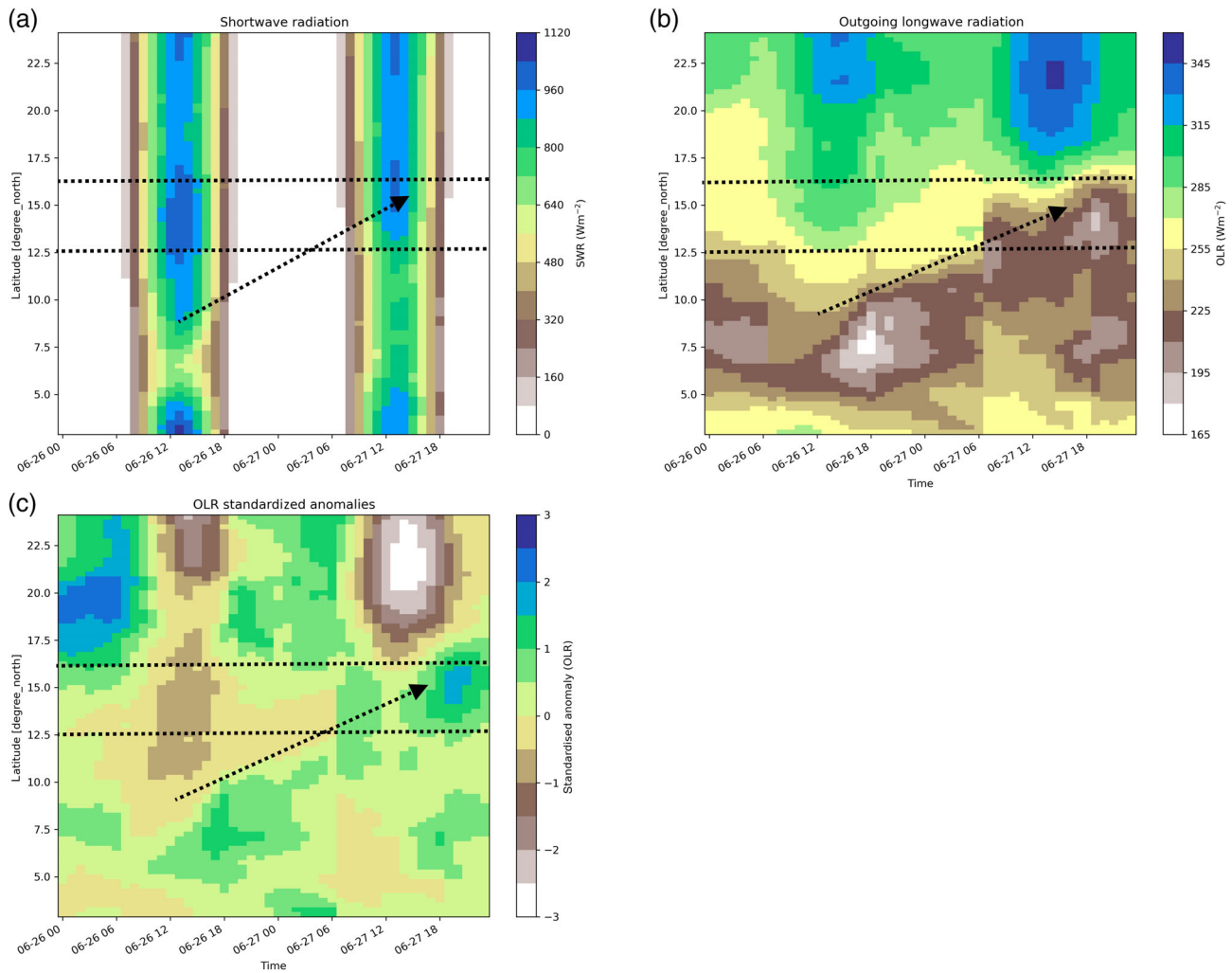
FIGURE 8 Time evolution of ERA5 top net shortwave radiation (a), outgoing longwave radiation (b) and the hourly standardized anomaly of the longwave radiation (c) averaged over longitudes 18.5°W to 3°E on 26–27 June 2018. The dashed black arrow indicates the propagation track, whereas the dashed zonal lines indicate the latitudinal region of storm 1 impact. All times have units in the Universal Time Coordinate (UTC).

intensified into a series of convective storms over southern Ghana, persisting through to 1800 UTC. The storm finally decayed between 2100 UTC on 28 June and 0000 UTC on 29 June 2018.

3.4.1 | Equivalent potential temperature

On 27 June, it is important to note that, the area of theta-e maxima (orange rectangle in Figure S2a,b), by midnight of 28 June, was a convergence zone of active storms (not shown). As this organized active storm decayed at around 1200 UTC (not shown), cold dry winds were expelled at 850 hPa, which lowered the theta-e (orange box, Figure 10b) to about 4σ below normal (Figure 10e). The emanating cold winds had anomalously strong speeds of around 4 ms^{-1}

(Figure 10e). Over West Africa, the mid-troposphere (500 hPa), is usually dry and cold due to the prevalent easterly winds from the AEJ. However, on 28 June, winds at 500 hPa, over Ghana (below 7°N in black box) were characterized by moderately strong moisture-laden southeasterlies, which changed to easterlies further north (Figure 10c). The result of the moisture-laden southeasterlies below 7°N (Figure 10c) and the anomalous windspeed (Figure 10f) was an increase in theta-e from 330 K on 27 June (see Figure S2c) to about 342 K (Figure 10c).

3.4.2 | Diurnal evolution of atmospheric controls

The NLLJ observed in Figure 6 on 27 June persists through to 28 June with a core of zonal wind flow of
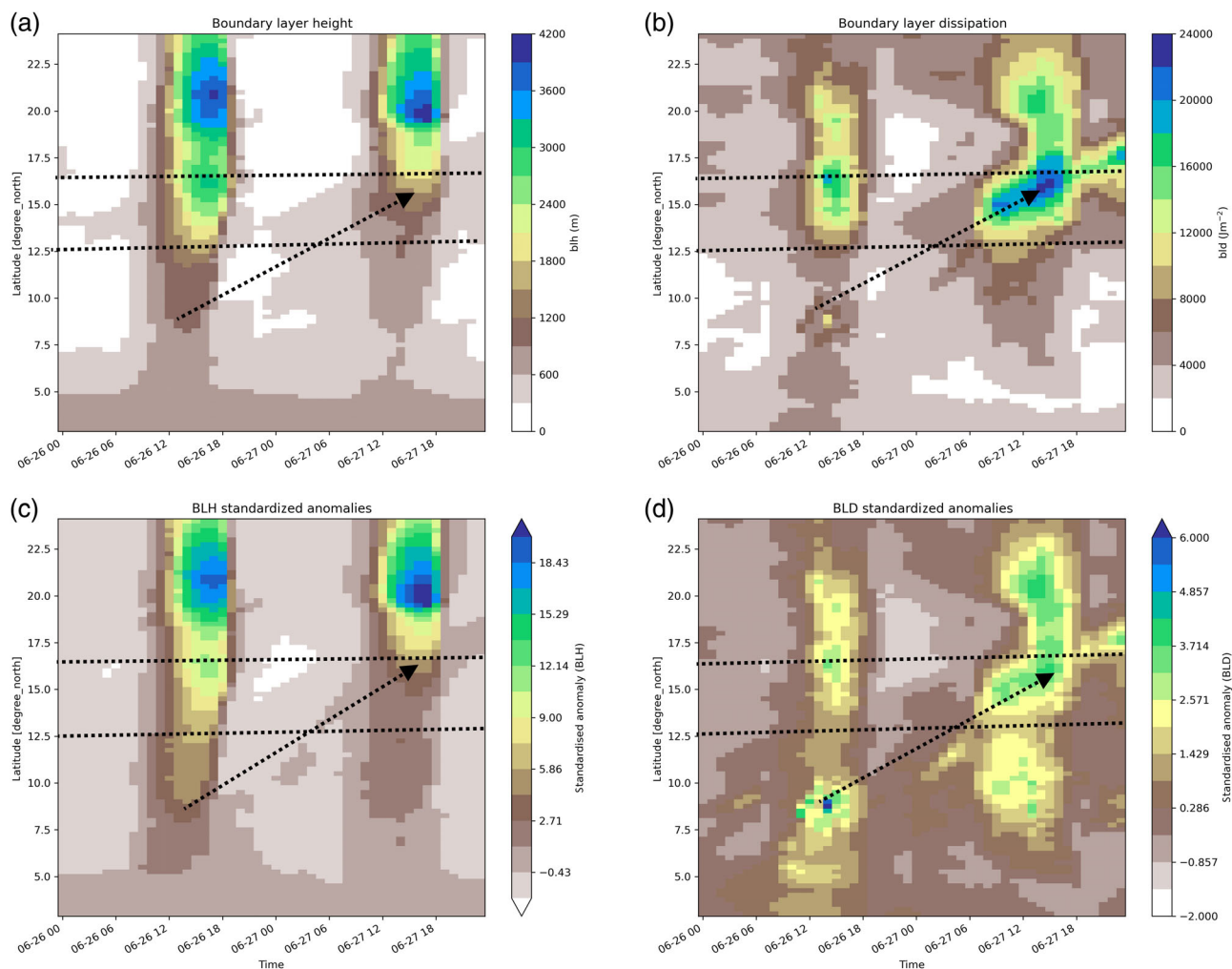
FIGURE 9 Hovmoller of ERA5 (a) boundary layer height (BLH) and (b) boundary layer dissipation (BLD), averaged over longitudes 18.5°W to 3°E on 26–27 June 2018. Panels (c) to (d) represent the corresponding hourly standardized anomalies from the 1981 to 2018 climatology. Dashed black arrow indicates the propagation track, whereas the dashed zonal lines indicate the latitudinal region of storm 1 impact. All times have units in the Universal Time Coordinate (UTC).

approximately 5 ms^{-1} between 0300 and 0600 UTC (Figure 11a). The low-level air (below 800 hPa) was also close to saturation (80%–100%) in the afternoon (1200–1500 UTC, Figure 11a) when storm initiated over southern Ghana. The specific humidity was especially high at the surface (1000 hPa; Figure 11b), although this was normal (Figure 11d). At the mid-troposphere (700–500 hPa), the lower than normal RH (Figure 11c) is significant for the development of the storm through evaporative cooling from downdraughts (Parker & Diop-Kane, 2017). Similar to storm 1, strong vertical ascent (Figure 12a) characterized the storm initiation and maturity periods (1200–1800 UTC), with the vertical mixing reaching up to the middle troposphere (500 hPa; Figure 12b). The cloud liquid water (Figure 12c) content was high throughout the day at the lower troposphere (below 800 hPa), with a peak in ice content during the

growth and maturity of the storm between 1200 and 1800 UTC (300–150 hPa; Figure 12d).

3.4.3 | Net radiation and boundary layer dynamics

The radiation dynamics for storm 2 is shown in Figure 13. Maximum SWR occurred at 1300 UTC (Figure 13a), with a corresponding BLH and dissipation peaking at 1400 UTC (Figure 14a,b). With sufficient energy dissipation, deep convection peaked after 1500 UTC (<210 Wm^{-2}; Figure 13b), when convective cells became fully matured (Figure S3). The anomalies in OLR were found to be higher than normal (1–1.5σ) during the storm evolution (Figure 13c). At the onset of convection, the height of the boundary layer deepened from 500 m at 0900 UTC to

FIGURE 10 ERA5-derived equivalent potential temperature overlaid with wind (a–c) vectors for 28 June 2018 and their standardized anomalies (d–f) at 1200 UTC. Black box shows the area of storm initiation, growth and impact, which is the southern region of Ghana. Orange box represents the area of high theta-e on 27 June at 1200 UTC as observed in Figure S2.
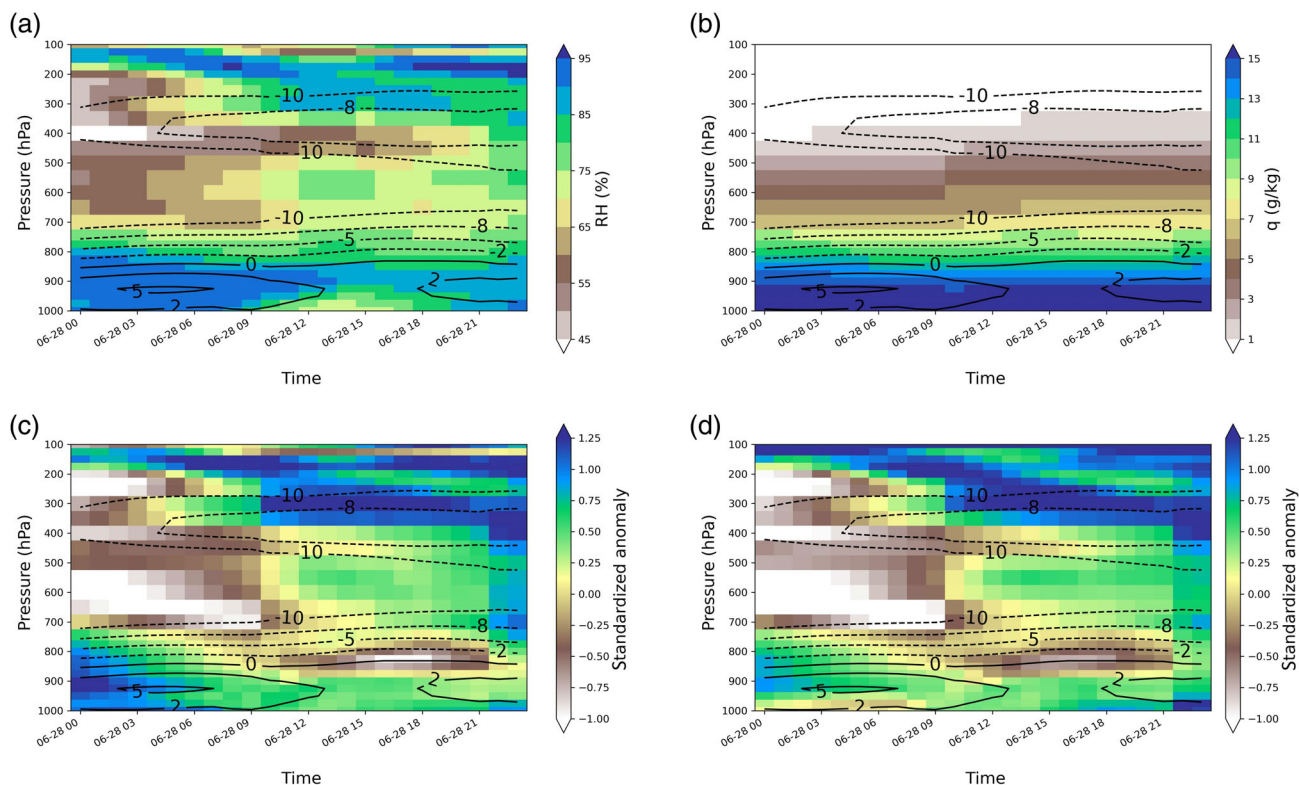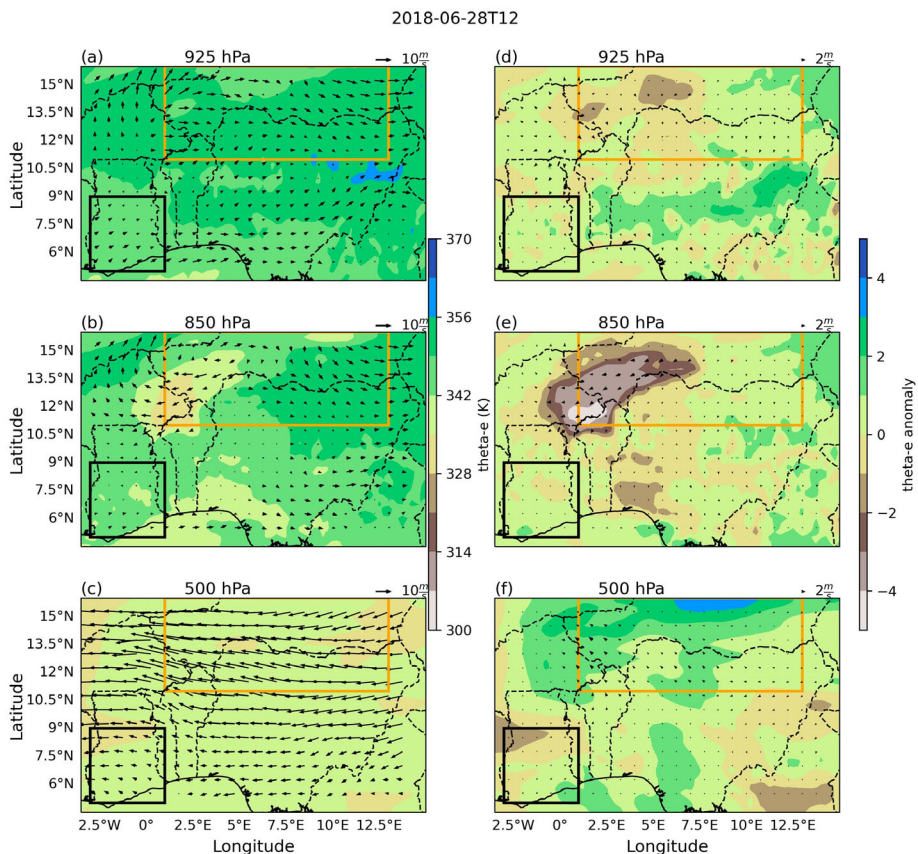

FIGURE 11 ERA5 diurnal vertical cross-section (a) relative humidity, (b) specific humidity (c) hourly standardized anomaly of relative humidity and (d) hourly standardized anomaly of specific humidity averaged over longitudes 3.5°W to 1.5°E and latitudes 4.5°N to 11.5°N for 28 June 2018. Overlay of contour lines shows the zonal wind components. All times have units in the Universal Time Coordinate (UTC).
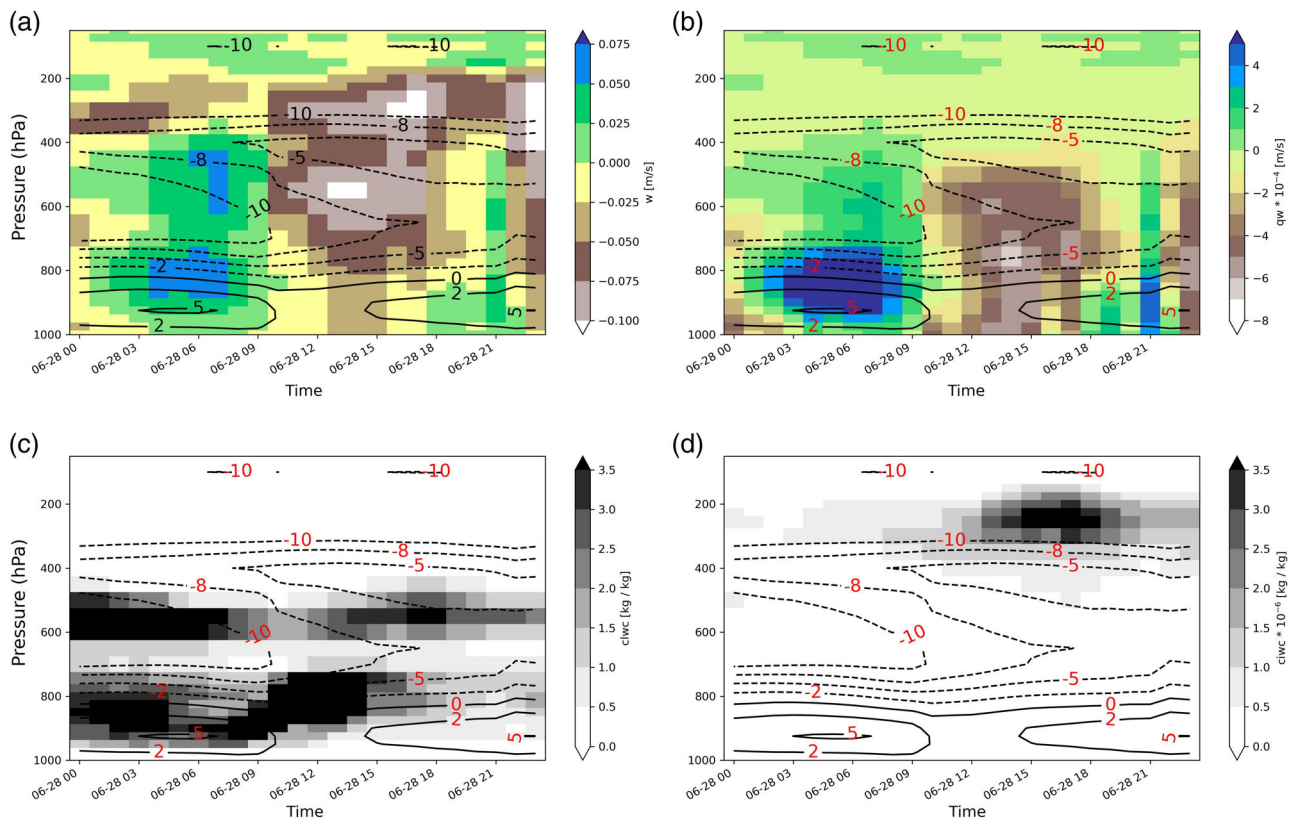
FIGURE 12 ERA5 diurnal vertical cross-section (a) vertical velocity (w), (b) vertical mixing (qw), (c) cloud liquid water content (*clwc*) and (d) cloud ice water content (*ciwc*) averaged over longitudes 3.5°W to 1.5°E and latitudes 4.5°N to 11.5°N for 28 June 2018. Overlay of contour lines represents the zonal wind components. Negative vertical velocity denotes ascent of air, whereas positive values indicate subsidence. Additionally, the vertical mixing (b) is the product of the specific humidity and vertical velocity and shows the depth of ascent or descent of moisture in the troposphere. All times have units in the Universal Time Coordinate (UTC).

about 1200 m by 1500 UTC (Figure 14a). The corresponding energy dissipation (Figure 14b) was between 3000 and 5000 Jm^{-2}, specifically over southern Ghana (6°N–9°N). The anomalies in BLH and energy dissipation were higher than normal at 4σ and 1σ, respectively (Figure 14c,d), which supported storm growth.

4 | DISCUSSIONS

4.1 | Storm 1: 26–27 June 2018

According to Scorer (1949) and Barry (1992), a strong decay of I^2 with height, especially at the mid-troposphere, is an indication of the potential for trapped waves. The smaller the Scorer parameter the easier waves are formed, leading to horizontal propagation of these trapped waves (see Sachsperger et al. (2015)). These dynamics can be observed in the decay of I^2 with height in Figure 4c. Although further numerical simulations are needed, from the satellite imagery (Figure 3), the trapped gravity wave may have formed from the parent storm

through the known downward reflection and resonance of vertically propagating waves (Howard, 2013). In addition, the presence of a low-level jet such as the AEJ, served as a significant barrier for the trapping of the waves, aided by the increasing mean windspeed (U), and a strong decay of the $\frac{d^2U}{dz^2}$ term with height (not shown). In an environment of sufficient moisture (as observed in Figure 2), the trapped wave acted to modify boundary layer processes to promote the initiation of severe convection and the growth and longevity of the thunderstorms on 26 June 2018, similar to findings by Howard (2013); Sachsperger et al. (2015); Stephan et al. (2021). The rear of the propagating gravity wave was a significant region for storm initiation (Figure 3), through the modification of tropospheric heating (Halliday et al., 2018). This heating can be envisaged in the higher than normal BLH and dissipation, occurring over the initiation zone. Moreover, an increase in low-level vertical ascent occurring in a trapped gravity wave can trigger deep convection (Emanuel et al., 1994). The vertical ascent over the Ghana–Togo ranges at 1000–925 hPa (not shown) showed high vertical ascent from 0600 to 1200 UTC, just about
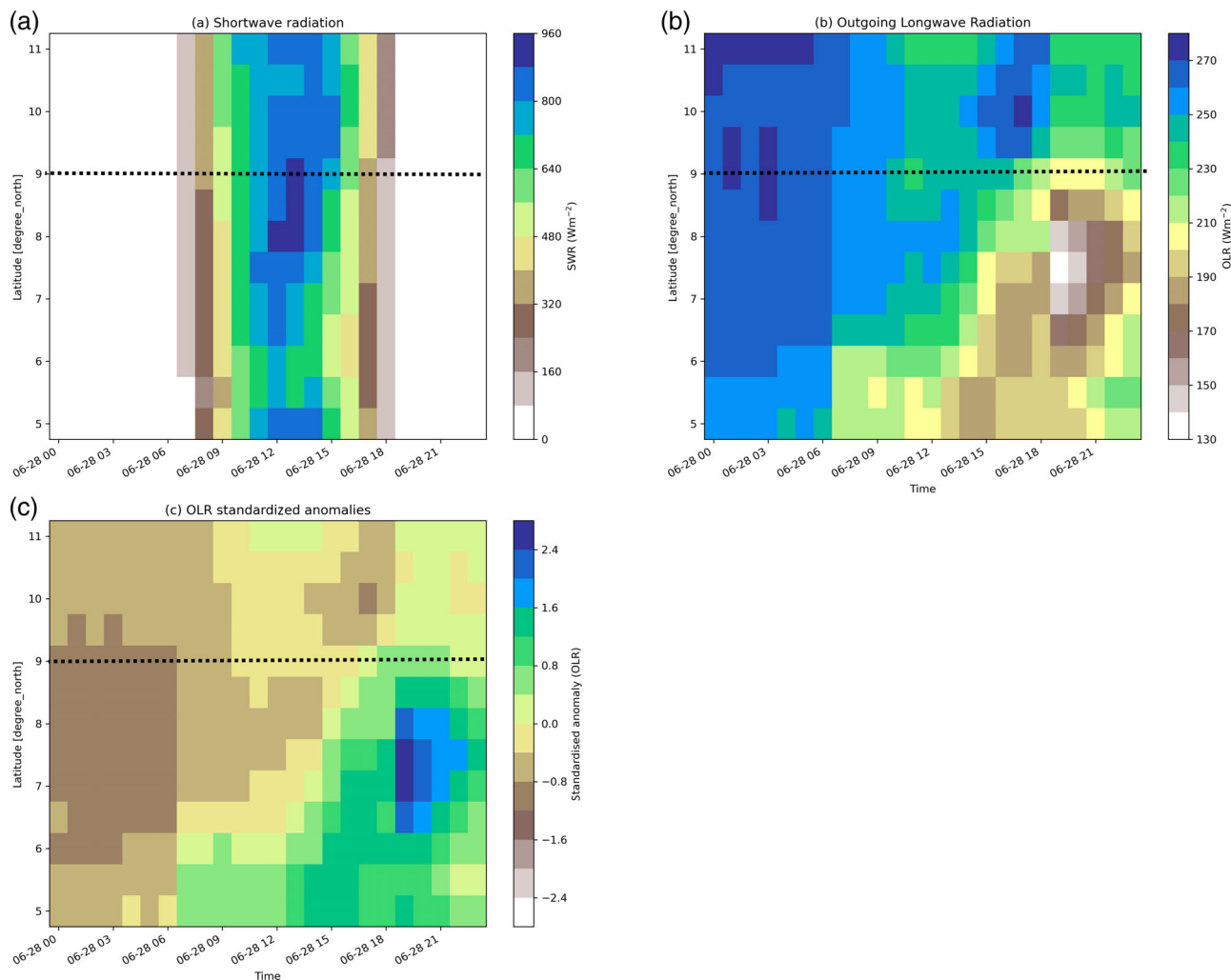
FIGURE 13   Time evolution of ERA5 top net shortwave (a) and outgoing longwave (b) radiations averaged over longitudes 3.5°W to 1.5°E for 28 June 2018. The hourly standardized anomalies for the outgoing longwave radiation are shown in panel (c). Storm 2 initiated south of the black dashed horizontal line at latitude 9°N. All times have units in the Universal Time Coordinate (UTC).

the time of wave passage. This strong vertical ascent, coupled with both monsoonal and Volta river moisture influx, and lift from the mountains, triggered the deep convection at 1200 UTC (shown by the four convective cells in Figure 3c).

Sufficient low-level moisture influx also increased the instability of the atmosphere as evident from the equivalent potential temperature (Figure 5a-c). Although the high theta-e over storm initiation region (around 8°N) at 925 hPa and 850 hPa on 26 June was normal (Figure 5a,b,d,e), it was significant for storm development due to the lift mechanism provided by the Ghana–Togo mountainous ranges. At the time of convection initiation on 26 June, strong deep convection characterized 8°N (OLR; ≈ 180 Wm^{-2}, Figure 8b), due to cloud-ice reflectance from the growing cumulonimbus clouds (see Figure 3d). The deep convective state over the initiation region was also accompanied by anomalously high BLH (5σ; Figure 9c) and boundary layer

energy dissipation (2–3σ; Figure 9d), possibly at the rear of the propagating trapped gravity wave. The energy dissipation was further enhanced by moderate vertical ascent within the same time period (see Figure 7a). In addition, the OLR (>240 Wm^{-2}) over the Saharan region ($>18°$N) is indicative of a warmer and drier air layer. This warm, dry air may have contributed to increased storm intensity over Senegal on 27 June, as they were advected by northeasterly winds at 925 hPa (see Figure 2b), creating dust plumes, which act as cloud condensation nuclei (CCN) for storm growth. In fact, according to Senghor et al. (2021), dust plumes of approximately 5 km vertical height, developed on the 26 June, and were strongly linked to the initiation of daughter storm cells over north-eastern Mali at 1600 UTC on the same day. For the dust to act as a CCN, the supply of moisture needed for condensation may have originated from the prevailing storm, as well as the weak westerlies over Senegal at 925 hPa on 27 June (see Figure 2b). Studies
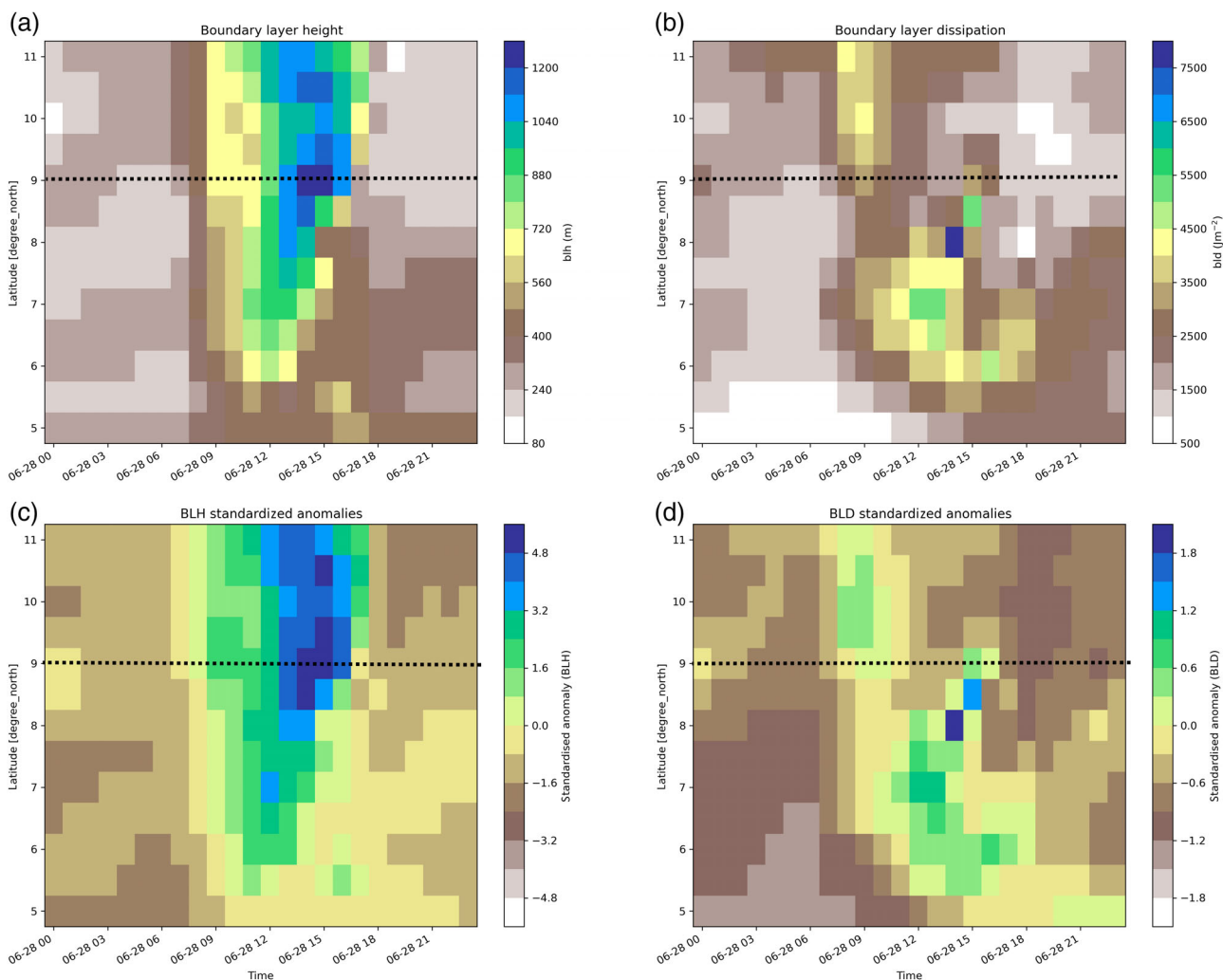
FIGURE 14 Time evolution of ERA5 (a) boundary layer height (BLH) and (b) boundary layer dissipation (BLD) averaged over longitudes 3.5°W to 1.5°E for 28 June 2018. Panels (c) and (d) show the corresponding hourly standardized anomalies associated with the boundary layer height and dissipation. Storm 2 initiated south of the black dashed horizontal line at latitude 9°N. All times have units in the Universal Time Coordinate (UTC).

have found that these westerlies are actually the West African westerly jet (WAWJ), which develops in early June, dissipates in mid-October and have speeds between 1.5 and 6 ms^{-1} (Liu et al., 2020; Pu & Cook, 2010). The jet plays a critical role by advecting moisture from the East Atlantic into the Sahelian region (0°W–10°W, 8°N–18°N). Furthermore, the associated moisture flux of the jet is usually significantly greater than that of the southerly flow of the WAM during this period (Liu et al., 2020).

4.2 | Storm 2: 28 June 2018

For storm initiation on 28 June, moisture depth over southern Ghana was enhanced by the strong southwesterlies at 600 hPa (Figure 2i) and southeasterlies at

500 hPa (Figure 10c). Cold winds from the previous organized convective cell, increased instability at the south of Ghana (high theta-e around 340–350 K), as it mixed with the weak to moderate southwesterlies at 850 hPa (Figure 10b). The anomalous cold theta-e region at 850 hPa also reflected an isolated dry punch found at the same level in Figure 2f. The BLH was anomalously high during storm initiation, accompanied by the anomalously high energy dissipation (Figure 14). The NLLJ had a stronger influence on the formation of storm 2, as its strength increased from 2 ms^{-1} on 27 June to 5 ms^{-1} on 28 June. The NLLJ is known to destabilize the lower troposphere and enhances the formation of low-level clouds such as stratus and stratocumulus in the presence of sufficient moisture supply (Aryee et al., 2021; Schrage & Fink, 2012; Schuster et al., 2013). Its role in advecting

moisture led to anomalous moistening of the surface (1000 hPa) to about 800 hPa between 0000 and 0900 UTC, edging the air closer to saturation (Figure 11a,c). At the same period, mid-levels (700–400 hPa) were drier, owing to an enhanced subsidence (Figure 12a), which restricted vertical mixing close to the surface (Figure 12b). As convection began from 1200 UTC, the strong vertical mixing (Figure 12b), moistened slightly the mid-troposphere (up to 500 hPa), which was still dry enough for evaporative cooling as the storm matured. The cloud liquid water and ice content increased to reflect the growth and maturity of the storm.

Another factor, although not fully explored in this study, is the influence of vegetation cover dynamics on MCS initiation, as found by Hartley et al. (2016). We hypothesize that this phenomenon might be prominent in the formation of the 28 June 2018 storm. According to Hartley et al. (2016), 33.8% of convective initiations occur over tree–grass boundaries. Furthermore, when an MCS simultaneously covers grass boundary and tree cover, the most intense rainfall occurred over forest cover 48.4% of the time, indicating that the moisture supplied by tree cover provides positive feedback to the rainfall. Their findings can be observed in Figure S3 of this study. For instance, the northern part of Ghana has sparse grassland vegetation, whereas moving south, the land cover is that of the deciduous and semi-deciduous forests. From Figure S3, it can be observed that at 1200 UTC, the decaying southern branch of the active storm over Burkina Faso propagated southward over Ghana. No initial intensification of the storm was observed at this time (1200 UTC). However, at 1500 UTC, we observe an intensification of the storm due to the initiation of several convective cells that appeared along the propagation track. The merging of the cells intensified the storm over the entire middle to southern Ghana at 1800 UTC. Hence the vegetation cover likely played a critical role in storm intensification on 28 June from the middle sector of the country to the coast, while a stable environment presided over the north.

5 | CONCLUSIONS

Mesoscale convective systems (MCSs) account for nearly 70% of the rainfall in West Africa. Forecasting these systems over the region is still challenging due to the complex interaction between synoptic, local and atmospheric dynamics. Their propagation over the region is usually associated with devastations to lives and properties. Therefore, understanding the environmental evolution of MCSs is critical for forecasting weather in the West

African sub-region. This study focused on investigating the thermodynamic and synoptic environments leading to the formation of two MCSs over West Africa on 26 (storm 1) and 28 (storm 2) June 2018. Primary datasets used to assess the diurnal evolution of the storms were obtained from ERA5.

Based on the analysis of the Scorer Parameter and Brunt–Vaisala frequency, the results showed that a propagating trapped gravity wave, enhanced by the African Easterly Jet (AEJ), likely played a role in the initiation of storm 1 on 26 June over the mountainous Ghana–Togo ranges. Also, on 26 June, the AEJ was established with maximum winds of 10 ms^{-1}, and a significant MT located south of the jet core. For the initiation of both storms, several cyclonic and anti-cyclonic vortices, which formed at the lower (925–850 hPa) and middle (600 hPa) troposphere, controlled moisture influx into the region. The West African westerly jet (WAWJ) was also present on 27 June at 1200 UTC to aid westerly moisture advection into the storm at the region of impact. For storm 2, the NLLJ influenced low-level (1000–925 hPa) moisture advection, as jet speed increased to 5 ms^{-1}. This may have led to the anomalous high lower tropospheric saturation and specific humidity. Strong subsidence from 1000 to 400 hPa in the early morning restricted vertical mixing and turbulence close to the surface. However, at the onset of convection, vertical mixing and turbulence moistened the middle troposphere to enhance storm growth. For storms 1 and 2, the evolution of the OLR indicated an established region of consistent deep convection from storm initiation to decay. BLH increased significantly on the initiation of both storms to support increasing warm air ascent.

Over West Africa, the dynamics of gravity waves emanating from existing storms are usually not analysed by weather forecasters. Few models such as the Met Office Unified Model have accurately represented gravity wave impact on secondary convection initiations over the region (Birch et al., 2013). An inclusion of these wave dynamics into numerical weather prediction models at operational centres would be very much needed for afternoon nowcasting in the region. For a propagating gravity wave, regions at its rear and dissipation are high-likelihood sources for storm initiations during the summer monsoon. West African forecasters must therefore monitor wave activities in the region from decaying storms, especially in the early morning, to increase the accuracy of afternoon storm initiation nowcasts. In addition, coupling the propagation of the waves with the model prognosis of the atmosphere and land-surface dynamics during the day would increase considerably the accuracy of forecasting storm events over the region. Under the GCRF African Science for

Meteorological Applications
Science and Technology for Weather and Climate · Open Access · RMetS

Weather Information and Forecasting Techniques (SWIFT), these findings are crucial in fulfilment of the project's aim to improve weather forecasting capability and communication over West Africa.

AUTHOR CONTRIBUTIONS

ACKNOWLEDGEMENTS

CONFLICT OF INTEREST
The authors declare no conflicts of interest.

DATA AVAILABILITY STATEMENT
All datasets used in this study are freely available online at their individual websites.

ORCID
Marian Amoakowaah Osei https://orcid.org/0000-0003-3481-7222
Jeffrey N. A. Aryee https://orcid.org/0000-0002-4481-1441
Jacob Agyekum https://orcid.org/0000-0001-7484-5338
Samuel Owusu Ansah https://orcid.org/0000-0001-5375-8876
Frank Baffour-Ata https://orcid.org/0000-0002-6363-732X
Leonard K. Amekudzi https://orcid.org/0000-0002-2186-3425
Winifred Ayinpogbilla Atiah https://orcid.org/0000-0003-3409-2380
Michael Padi https://orcid.org/0000-0001-8523-4110
Johnson Ameho https://orcid.org/0000-0002-9857-8980
Bashiru Yahaya https://orcid.org/0000-0001-8754-100X

REFERENCES

Akinyemi, D.F., Ayanlade, O.S., Nwaezeigwe, J.O. & Ayanlade, A. (2019) A comparison of the accuracy of multi-satellite precipitation estimation and ground meteorological records over Southwestern Nigeria. *Remote Sensing in Earth Systems Sciences*, 3, 1–12.

Aryee, J.N., Amekudzi, L.K. & Yamba, E.I. (2021) Low-level cloud development and diurnal cycle in Southern West Africa during the DACCIWA field campaign: case study of Kumasi Supersite, Ghana. *Journal of Geophysical Research: Atmospheres*, 126, e2020JD034028.

Atiah, W.A., Amekudzi, L.K., Aryee, J.N.A., Preko, K. & Danuor, S.K. (2020) Validation of satellite and merged rainfall data over Ghana, West Africa. *Atmosphere*, 11, 859.

Atiah, W.A., Tsidu, G.M. & Amekudzi, L.K. (2020) Investigating the merits of gauge and satellite rainfall data at local scales in Ghana, West Africa. *Weather and Climate Extremes*, 30, 100292.

Baidu, M., Schwendike, J., Marsham, J.H. & Bain, C. (2022) Effects of vertical wind shear on intensities of mesoscale convective systems over West and Central Africa. *Atmospheric Science Letters*, 23, e1094.

Barry, R.G. (1992) *Mountain weather and climate*. London: Psychology Press.

Bickle, M., Marsham, J.H., Griffiths, S.D., Ross, A.N. & Crook, J. (2022) The influence of the diurnal cycle in wind shear and thermodynamics on squall lines in the West African Monsoon. *Journal of the Atmospheric Sciences*, 79, 2125–2143.

Birch, C., Parker, D., O'Leary, A., Marsham, J., Taylor, C., Harris, P. et al. (2013) Impact of soil moisture and convectively generated waves on the initiation of a West African mesoscale convective system. *Quarterly Journal of the Royal Meteorological Society*, 139, 1712–1730.

Copernicus Climate Change Service (C3S). (2017) *ERA5: fifth generation of ECMWF atmospheric reanalyses of the global climate*. Available at: https://cds.climate.copernicus.eu/cdsapp [Accessed 03th February 2020].

Crook, N.A. (1988) Trapping of low-level internal gravity waves. *Journal of Atmospheric Sciences*, 45, 1533–1541.

Dembélé, M. & Zwart, S.J. (2016) Evaluation and comparison of satellite-based rainfall products in Burkina Faso, West Africa. *International Journal of Remote Sensing*, 37, 3995–4014.

Dieng, A.L., Eymard, L., Sall, S.M., Lazar, A. & Leduc-Leballeur, M. (2014) Analysis of strengthening and dissipating mesoscale convective systems propagating off the West African coast. *Monthly Weather Review*, 142, 4600–4623.

Emanuel, K.A., David Neelin, J. & Bretherton, C.S. (1994) On large-scale circulations in convecting atmospheres. *Quarterly Journal of the Royal Meteorological Society*, 120, 1111–1143.

Fontaine, B., Louvet, S. & Roucou, P. (2008) Definition and predictability of an OLR-based West African monsoon onset. *International Journal of Climatology: A Journal of the Royal Meteorological Society*, 28, 1787–1798.

Funk, C., Peterson, P., Landsfeld, M., Pedreros, D., Verdin, J., Shukla, S. et al. (2015) The climate hazards infrared precipitation with stations—a new environmental record for monitoring extremes. *Scientific Data*, 2, 1–21.

Gu, L., Meyers, T., Pallardy, S.G., Hanson, P.J., Yang, B., Heuer, M. et al. (2006) Direct and indirect effects of atmospheric conditions and soil moisture on surface energy partitioning revealed by a prolonged drought at a temperate forest site. *Journal of Geophysical Research: Atmospheres*, 111, 1–13.

Halliday, O.J., Griffiths, S.D., Parker, D.J., Stirling, A. & Vosper, S. (2018) Forced gravity waves and the tropospheric response to convection. *Quarterly Journal of the Royal Meteorological Society*, 144, 917–933.

Hartley, A.J., Parker, D.J., Garcia-Carreras, L. & Webster, S. (2016) Simulation of vegetation feedbacks on local and regional scale precipitation in West Africa. *Agricultural and Forest Meteorology*, 222, 59–70.

Hersbach, H., Bell, B., Berrisford, P., Hirahara, S., Horányi, A., Muñoz-Sabater, J. et al. (2020) The ERA5 global reanalysis. *Quarterly Journal of the Royal Meteorological Society*, 146, 1999–2049.

Houze, R.A., Jr. (2004) Mesoscale convective systems. *Reviews of Geophysics*, 42, 1–43.

Howard, B.B. (2013) *Severe convective storms and tornadoes. Observations and dynamics*. Heidelberg: Springer-Verlag Berlin.

Kafando, P., Chane-Ming, F. & Petitdidier, M. (2008) Climatology of gravity wave activity during the West African Monsoon. *Annales Geophysicae*, 26, 4081–4089.

Kalashnik, M. (2013) Propagation and trapping of inertial gravity waves in shear flows (ray theory). *Izvestiya, Atmospheric and Oceanic Physics*, 49, 217–228.

Klein, C., Nkrumah, F., Taylor, C.M. & Adefisan, E.A. (2021) Seasonality and trends of drivers of mesoscale convective systems in southern West Africa. *Journal of Climate*, 34, 71–87.

Klein, C. & Taylor, C.M. (2020) Dry soils can intensify mesoscale convective systems. *Proceedings of the National Academy of Sciences*, 117, 21132–21137.

Liu, W., Cook, K.H. & Vizy, E.K. (2020) Role of the West African westerly jet in the seasonal and diurnal cycles of precipitation over West Africa. *Climate Dynamics*, 54, 843–861.

May, R.M., Arms, S.C., Marsh, P., Bruning, E., Leeman, J.R., Goebbert, K. et al. (2022) *Metpy: a Python package for meteorological data*. Available at: https://github.com/Unidata/MetPy

McKee, T.B., Doesken, N.J. & Kleist, J. (1993) The relationship of drought frequency and duration to time scales. In: *Proceedings of the 8th conference on applied climatology*, Vol. 17. Boston, MA: American Meteorological Society, pp. 179–183.

Oduro-Afriyie, K. (1989) On the mean monthly equivalent potential temperature and rainfall in West Africa. *Theoretical and Applied climatology*, 39, 188–193.

Parker, D.J. & Diop-Kane, M. (2017) *Meteorology of tropical West Africa: the forecasters' handbook*. West Sussex, UK: John Wiley & Sons.

Peterson, P., Funk, C., Husak, G., Pedreros, D., Landsfeld, M., Verdin, J. et al. (2013) The Climate Hazards group InfraRed Precipitation (CHIRP) with Stations (CHIRPS): development and validation. In: *AGU Fall meeting abstracts*. Massachusetts: SAO/NASA Astrophysics Data System. https://ui.adsabs.harvard.edu/abs/2013AGUFM.H33E1417P

Plougonven, R. & Snyder, C. (2005) Gravity waves excited by jets: propagation versus generation. *Geophysical Research Letters*, 32, 1–4.

Pu, B. & Cook, K.H. (2010) Dynamics of the West African westerly jet. *Journal of Climate*, 23, 6263–6276.

Sachsperger, J., Serafin, S. & Grubišić, V. (2015) Lee waves on the boundary-layer inversion and their dependence on free-atmospheric stability. *Frontiers in Earth Science*, 3, 70.

Schrage, J.M. & Fink, A.H. (2012) Nocturnal continental low-level stratus over tropical West Africa: observations and possible mechanisms controlling its onset. *Monthly Weather Review*, 140, 1794–1809.

Schrage, J.M., Fink, A.H., Ermert, V. & Ahlonsou, E.D. (2006) Three MCS cases occurring in different synoptic environments in the sub-Sahelian wet zone during the 2002 West African monsoon. *Journal of the Atmospheric Sciences*, 63, 2369–2382.

Schuster, R., Fink, A.H. & Knippertz, P. (2013) Formation and maintenance of nocturnal low-level stratus over the southern West African monsoon region during AMMA 2006. *Journal of the Atmospheric Sciences*, 70, 2337–2355.

Scorer, R.S. (1949) Theory of waves in the lee of mountains. *Quarterly Journal of the Royal Meteorological Society*, 75, 41–56.

Senghor, H., Roberts, A.J., Dieng, A.L., Wane, D., Dione, C., Fall, M. et al. (2021) Transport and deposition of Saharan dust observed from satellite images and ground measurements. *Journal of Atmospheric Science Research*, 4, 1–11.

Stephan, C.C., Žagar, N. & Shepherd, T.G. (2021) Waves and coherent flows in the tropical atmosphere: new opportunities, old challenges. *Quarterly Journal of the Royal Meteorological Society*, 147, 2597–2624.

Taylor, C.M. (2008) Intraseasonal land–atmosphere coupling in the West African monsoon. *Journal of Climate*, 21, 6636–6648.

Taylor, C.M., Belušić, D., Guichard, F., Parker, D.J., Vischel, T., Bock, O. et al. (2017) Frequency of extreme Sahelian storms tripled since 1982 in satellite observations. *Nature*, 544, 475–478.

Taylor, C.M., Harris, P.P. & Parker, D.J. (2010) Impact of soil moisture on the development of a Sahelian mesoscale convective system: a case-study from the AMMA special observing period. *Quarterly Journal of the Royal Meteorological Society*, 136, 456–470.

Vizy, E.K. & Cook, K.H. (2018) Mesoscale convective systems and nocturnal rainfall over the West African Sahel: role of the Inter-tropical front. *Climate Dynamics*, 50, 587–614.

Wallace, J.M. & Hobbs, P.V. (2006) *Atmospheric science: an introductory survey*, Vol. 92. New York: Elsevier.

Wang, S., Zhang, F. & Snyder, C. (2009) Generation and propagation of inertia–gravity waves from vortex dipoles and jets. *Journal of the Atmospheric Sciences*, 66, 1294–1314.

SUPPORTING INFORMATION

Additional supporting information can be found online in the Supporting Information section at the end of this article.